Structural and Quantum Chemical Studies of 8-Aryl-sulfanyl Adenine Class Hsp90 Inhibitors[†]

Robert M. Immormino,[‡,§] Yanlong Kang,[ǁ] Gabriela Chiosis,[ǁ] and Daniel T. Gewirth*,[‡,§]

Hauptman-Woodward Medical Research Institute, Buffalo, New York 14203, Department of Biochemistry, Duke University Medical Center, Durham, North Carolina 27710, and Department of Medicine, Program in Molecular Pharmacology and Chemistry, Memorial Sloan-Kettering Cancer Center, New York, New York 10021

Received March 15, 2006

Hsp90 chaperones play a critical role in modulating the activity of many cell signaling proteins and are an attractive target for anti-cancer therapeutics. We report here the structures of the water soluble 8-aryl-sulfanyl adenine class Hsp90 inhibitors, **1** (PU-H71) and **2** (PU-H64), in complex with the *N*-terminal domain of human Hsp90α. The conformation of **1** when bound to Hsp90 differs from previously reported 8-aryl adenine Hsp90 inhibitors including **3** (PU24FCl). While the binding mode for **3** places the 2′-halide of the 8-aryl group on top of the adenine ring, for **1** and **2**, we show that the 2′-halide is rotated approximately 180° away. This difference explains the opposing trends in Hsp90 inhibitory activity for the 2′-halo derivatives of the 3′,4′,5′-trimethoxy series where Cl > Br > I compared to the 4′,5′-methylenedioxy series where I > Br > Cl. We also present quantum chemical calculations of **2** and its analogues that illuminate their basis for Hsp90 inhibition. The calculated conformation of **2** agreed well with the crystallographically observed conformations of **1** and **2**. The predictive nature of the calculations has allowed the exploration of additional derivatives based on the 8-aryl adenine scaffold.

Introduction

Heat shock protein 90 (Hsp90) is an essential molecular chaperone[1,2] that requires ATP[3−5] for progression through its chaperone cycle. The Hsp90 chaperones, which include cytoplasmic Hsp90α and Hsp90β, endoplasmic reticulum GRP94, and mitochondrial TRAP-1, have three domains. ATP binding is localized to the *N*-terminal regulatory domain.[6,7] The *C*-terminal domain is responsible for homodimerization and contains the tetratricopeptide repeat (TPR), which is important for co-chaperone docking, and harbors a binding site for novobiocin.[8−10] Between these two domains is the middle domain, which stabilizes the *γ*-phosphate of ATP[11] and, in addition to the *N*-terminal domain, participates in the Hsp90 ATPase activity.[12]

Many proteins require Hsp90 for maturation or cellular regulation. Such clients include cell-cycle proteins such as Cdc2, Cdk4, Cdk6, and Cdk9, signaling kinases such as HRI, Raf-1, mutant p53, Akt, ErbB2, and Her2, and nuclear hormone receptors such as ER, AR, and GR.[13−15] The mutation or disregulation of these clients is buffered by Hsp90, which helps to maintain transformation and increases the rate of survival for cancer cells. The inhibition of Hsp90 ultimately leads to the degradation of client proteins via the ubiquitin proteasome pathway.[16,17] This leads to growth arrest and sensitization to further treatment for tumor cells in culture and tumor growth inhibition or regression in animal models.[13,18−20] As a key player in the activation of proteins important for cell cycle progression and tumerogenesis, Hsp90 is a promising target for anti-cancer therapeutics.

The anti-cancer activity of Hsp90 inhibitors has driven the discovery of many potent inhibitors including derivatives of the known natural product antibiotics geldanamycin,[21] radicicol,[22] and the natural ligand, ATP.[23−27] There is ongoing research into the development of more potent and efficacious Hsp90 inhibitors based both on the natural product leads and novel scaffolds. Among the geldanamycin derivatives, 17-allylamino,17-desmethoxy-geldanamycin (17-AAG) has advanced to clinical trials and has been shown to have selective affinity for Hsp90 isolated from tumor cells compared to Hsp90 derived from nontumor cells.[28] The derivatives of radicicol exploit the antibiotic's resorcinol ring, which makes direct contacts to Asp93 in human Hsp90[29] and appears to be critical to the binding mode. Recent reports have also highlighted radicicol−geldanamycin chimeras[30,31] and the diarylpyrazole class of ligands,[29,32,33] which also contain the resorcinol ring, as potent Hsp90 inhibitors. Finally, **3** (PU24FCl) and **4** (PU3)[23−26] or the 8-aryl-sulfanyl adenine derivates,[27] which include 8-(6-iodo-benzo[1,3]dioxol-5-ylsulfanyl)-9-(3-isopropyl-amino-propyl)-adenine, **1** (PU-H71) presented here, build upon a purine scaffold (Table 1, Figure 1).

Purine-based ligands including the −CH₂− linked **3** and the −S− linked **1** and **2** are 8-aryl adenine compounds that are designed to mimic the C-shape conformation adopted by ATP/ADP when bound to Hsp90.[34] The structures of several −CH₂− linked 8-aryl adenine compounds in complex with the *N*-terminal domain of human Hsp90α have been previously described.[23] In each case, the adenine moiety binds to the protein in a manner similar to that of ATP, while the substituted 8-aryl ring wedges between a lengthened Helix 3 and the core *β*-sheet. This ligand wedging creates a new binding channel that extends from the adenine-binding cavity behind Helix 3 and out into solvent. The formation of this channel requires a conformational change in the polypeptide loop that connects helices 3 and 4, resulting in a continuous helix, and moves residues 105−113 away from the adenine-binding cavity, thus interrupting packing interactions with the *β*-sheet. The structural characterization of this channel has shown that substitutions at the 4′ or 5′ positions of the phenyl ring are placed deeper in the channel.[23] Substitutions at the 2′ or 3′ positions, however, interact with

Table 1.

| cmpd	name	C2	R	L	X1	X3	IC$_{50}$ (nM)	PDB
1	PU-H71	H	3-isopropyl amino-propyl	S	I	4′,5′-methylenedioxy	50[36]	2FWZ[a]
2	PU-H64	H	3-isopropyl amino-propyl	S	Br	4′,5′-methylenedioxy	200[36]	2FWY[a]
3	PU24FCl	F	1-pentynyl	CH$_2$	Cl	3′,4′,5′-trimethoxy	1500[25,35]	1UYF[23]
4	PU3	H	*n*-butyl	CH$_2$	H	3′,4′,5′-trimethoxy	50000[17]	1UY6[23]
5	33	F	1-pentynyl	CH$_2$	Cl	4′,5′-dimethoxy	30000[36]	
	Comparison of Sulfur and oxidized linkers							
6	11w2	H	*n*-butyl	S	H	3′,4′,5′-trimethoxy	88500[35]	
7	27d	H	*n*-butyl	SO	H	3′,4′,5′-trimethoxy	110000[35]	
8	28d	H	*n*-butyl	SO$_2$	H	3′,4′,5′-trimethoxy	315000[35]	
	Model compounds used for quantum calculations							
9	8-sulfanyl	H	H	S	H	-	N/A	
10	8-sulfoxy	H	H	SO	H	-	N/A	
11	8-sulfonyl	H	H	SO$_2$	H	-	N/A	
12	8-PCA	H	H	CH$_2$	Br	4′,5′-dimethoxy	N/A	

[a] Structures presented in this work.
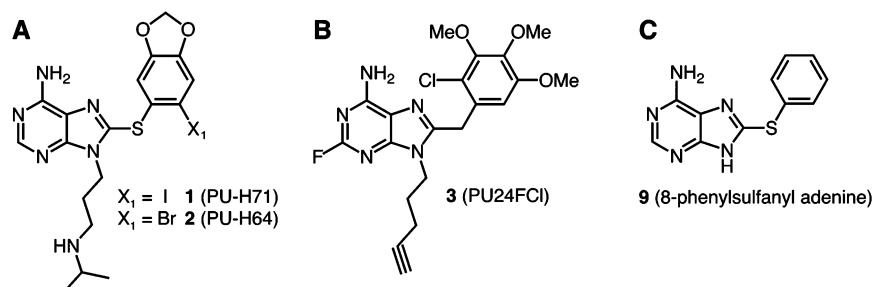
Figure 1. Purine based Hsp90 inhibitors and model compounds. (A) **1** (PU-H71) and **2** (PU-H64). The identity of the 2′-halide is indicated. (B) **3** (PU24FCl). (C) 8-phenylsulfanyl adenine, a model compound used for quantum chemical calculations.

the mouth of the channel and are in part responsible for the bond angle of the −CH$_2$− linker and the tilt of the phenyl ring. The linker between the adenine ring and the 8-aryl group, whether −CH$_2$− or −S−, is the other region that determines the position of the 8-aryl group in the cavity. No structure of an S-linked 8-aryl adenine compound in complex with Hsp90 has been described yet.

The study of the purine-based Hsp90 inhibitors promises to aid our understanding of their mechanism of inhibition and mode of interaction. Here, we present the structures of the novel S-linked adenine scaffold inhibitors **1** and **2** (Figure 1A) in complex with the *N*-terminal domain of human Hsp90α (PDB codes 2FWZ and 2FWY, respectively). Hsp90α was used for these studies to facilitate comparisons with structures of Hsp90α in complex with −CH$_2$-linked 8-aryl adenine inhibitors that were previously reported.[23] Our structural analysis of **1** and **2** highlights the key interactions conserved by all purine scaffold inhibitors and the unique interactions exploited by **1** and **2**. We also present quantum chemical calculations on a series of 8-aryl-sulfanyl adenine compounds. These analyses, coupled with the experimentally determined structure of the complex between **1** and Hsp90α, allow us to evaluate the effect of individual derivatizations on the 8-aryl group and explain the previously observed effects of oxidation at the sulfur linker.[35]

Results and Discussion

Crystallization and Structure Solution. The structures of the *N*-terminal domain of human Hsp90 in complex with **1** (PDB code 2FWZ) and **2** (PDB code 2FWY) were solved and refined at 2.1 Å resolution. The crystals of the complexes were grown in the presence of a 5-fold molar excess of the ligand. The structure of the complex with **1** was solved by single wavelength anomalous dispersion, exploiting the strong anomalous signal from the iodine atom at the 2′-position on the ligand. The structure with **2** was solved by molecular replacement using the structure of the human Hsp90 *N*-domain(PDB code 1UY6) as the search model. The final refined models have good electron density for all protein and ligand atoms. Data collection and structure refinement statistics are listed in Table 2.

Architecture of Binding. To explore the structural effects of the sulfur linker that distinguishes **1** from **3** and other −CH$_2$−linked inhibitors, we have solved the structure of the human Hsp90α *N*-terminal domain in complex with **1**. Figure 2A shows a stereoview of **1** in the ligand binding pocket of Hsp90, and the interactions are shown schematically in Figure 2B. The adenine moiety of **1** binds in a manner similar to that of ATP, maintaining the network of hydrogen bonds between the protein and the adenine portion of the ligand. In particular, the direct hydrogen bond from N6 on the adenine to Asp93 in Hsp90 is

Table 2. Summary of Data Collection and Refinement Statistics

diffraction data	hHsp90α+**1** (PU-H71)	hHsp90α+**2** (PU-H64)	yHsp90 + **2**
PDB code	2FWZ	2FWY	1ZW9
source	RaxisIV	RaxisIV	RaxisIV
space group	*I*222	*I*222	*P*4$_3$22
a, b, c (Å)	66.68, 91.28, 98.64	66.61, 90.59, 98.03	73.76, 73.76, 110.13
wavelength (Å)	1.54178	1.54178	1.54178
resolution (Å)[a]	50−2.1	50−2.1	50−1.9
(last shell) (Å)	2.18−2.1	2.18−2.1	1.97−1.9
unique reflections	33393	16139	24557
completeness (%)	98.2 (83.7)	91.4 (87.3)	99.6 (99.0)
average I/σ$_I$	15.5 (6.1)	31.7 (5.7)	16.6 (5.3)
redundancy	3.5	3.6	7.6
R_{sym}[b] (%)	4.4 (12.6)	3.6 (16.4)	7.3 (39.0)
resolution range (Å)	50−2.1	50−2.1	50−1.9
reflections (*F* > 2 σ$_F$)	33393	15965	24542
	(33319)	(15389)	(24353)
nonsolvent atoms	1631	1626	1633
solvent and heteroatoms	350	318	352
rmsd from ideality			
bond lengths (Å)	.0049	.0053	.0061
bond angles (°)	1.350	1.328	1.378
R[c] value (*F* > 2 σ$_F$) (%)	19.0 (18.9)	18.1 (17.7)	20.3 (20.0)
R[c]$_{free}$ (*F* > 2 σ$_F$) (%)	22.8 (22.7)	22.2 (21.7)	22.5 (22.4)
structure solution	SAD (iodine)	MR	MR
phasing power[d]	2.83		
FOM (after DM)[e,f]	.46 (0.95)		
all-atom clashscore (B < 40)[41]	8.21 (6.21)	8.22 (5.57)	5.47 (2.45)

[a] The resolution limit was defined as the highest resolution shell where the average I/σ$_I$ was >2 and data was reasonably complete. [b] $R_{sym} = \sum_{hkl}\sum_{ii(hkl)} - \langle I_{(hkl)}\rangle|/\sum_{hkl}\sum_i I_{(hkl)}$. [c] $R = ||F_o - F_c|/|F_o|$; ~10% of reflections were used to calculate R_{free}. [d] Phasing power = $[|F_H|/E]$, where E is the residual lack of closure. [e] Figure of merit = $|P(\alpha)e^{i\alpha}/P(\alpha)|$, where α is the phase, and $P(\alpha)$ is the phase probability distribution. [f] Figure of merit and phasing power were calculated to 4 Å. The density modification was preformed on the entire resolution range

preserved, as are the water-mediated hydrogen bonds to Leu48, Asn51, Ile91, Asp93, Gly97, and Thr184 and the hydrophobic contacts between Met 98 and Ala55 to the top and C2 side of the adenine ring.

In addition to these conserved contacts, the 8-aryl portion of **1** forms a new series of interactions with the protein. Compared to structures of the unliganded form of the Hsp90 N-domain, the binding of **1** (Figure 2C) requires a rearrangement of the loop joining helices 3 and 4 and the creation of a new binding channel that disrupts the packing interactions between helix 3 and the β-sheet core of Hsp90. A similar remodeling has also been observed for complexes between Hsp90 and other PU series ligands,[23] which bind to Hsp90 in a manner similar to that of **1**. Trp162 and Phe138 form the top and back of this predominantly hydrophobic channel and make edge-on-face and face-on-face π-stacking interactions, respectively, with the 8-aryl portion of **1**. The 8-aryl group also makes water-mediated hydrogen bonds from the iodine to the carbonyl oxygen of Leu107. The remaining interactions in the ligand binding pocket are a series of water-mediated hydrogen bonds that connect N3 to Asp102 (Figure 2A). The interactions between **2** and Hsp90 are similar to those seen for **1**, with the only significant difference being that an additional water is found near the 2′-bromo in **2**, which replaces the larger 2′-iodo in **1**.

The last unique derivatization of **1** and **2** is the amine-containing N9 alkane. The addition of an amine moiety improves the solubility of these compounds in aqueous solution while maintaining high affinity, potency, and oral availability.[36] This aqueous solubility distinguishes **1** and **2** from **4** and other purine-based inhibitors whose structures have been previously characterized.[23] The structure of the complex between **1** and Hsp90 reveals that the polar N9 amine makes no direct or water-mediated contacts to the protein but instead projects out into the solvent. This contrasts with derivatives of **4** that have nonpolar substituents at the N9 position, which exhibit bends in the N9 alkanes that keep the ends close to the surface of the

protein. The fact that the polar N9 side chain does not interact with the protein and projects into solvent suggests that this position is amenable to further modification that might improve the pharmacological properties of the compound.

To confirm the generality of the binding of **1** and **2** to Hsp90, we also determined the structure of yeast Hsp90 in complex with **2** (PDB code 1ZW9). Because all of the interactions seen in the structure of the complex of **2** with human Hsp90 were recapitulated in the structure of the complex of **2** with yeast Hsp90, the yeast complex will not be discussed further.

Effect of Halide Substitution at C2′ on the 8-Aryl Ring Orientation. Halide substitutions at the C2′ position of 3′,4′,5′-trimethoxy series ligands have been previously investigated.[23,26] These structure−activity studies showed that a 2′-chloro improves activity, as reported by geldanamycin competition binding assays for Hsp90 (EC$_{50}$) or IC$_{50}$ for Hsp90 degradation of Her2 in SKBr3 cells, whereas 2′-bromo had a slight negative effect.[26] The crystal structures of 2′-chloro-3′,4′,5′-trimethoxy compounds such as **3** in complex with human Hsp90α have shown that the 2′-halide sits on top of the adenine ring (Figure 2C) (for simplicity, referred to hereafter as s-cis) forming close van der Waals contacts in the ligand binding pocket.[23] These interactions explain the preference for the smaller 2′-chloro versus the 2′-bromo and suggest that the even larger 2′-iodo derivative would be inactive. Additionally, positioning the halide above the ring allows the N9-alkane to pack closely against the adenine, thus reducing the solvent exposed surface of this hydrophobic group.

In contrast to the halide preference for the 2′-halo-3′,4′,5′-trimethoxy derivatives, it has recently been reported that the halide preference for the 2′-halo-4′,5′-methylenedioxy series, of which **1** and **2** are members, is I > Br > Cl.[36] This preference order is exactly opposite that observed for the 2′-halo-3′,4′,5′-trimethoxy equivalents described above. This discovery led to the hypothesis that within the Hsp90 ligand binding pocket, the 8-aryl moiety of the 2′-halo-4′,5′-methylenedioxy series is
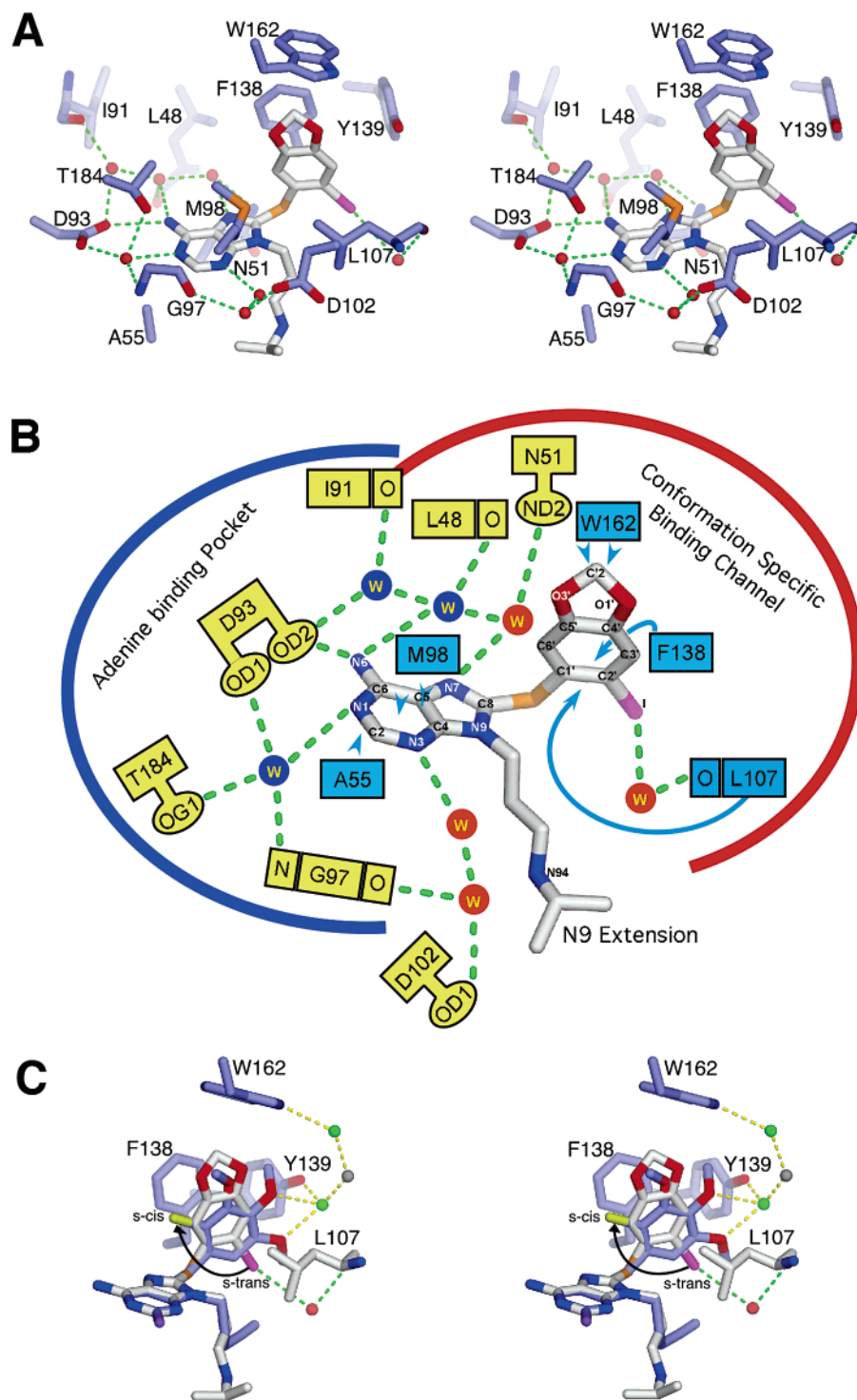
Figure 2. Interactions of Hsp90 with 1. (A) Stereo diagram of the Hsp90−1 interaction interface. Water molecules are represented as red spheres. Hydrogen bonds are represented as green dashed lines. (B) Schematic diagram of the protein−ligand interaction. The blue and red arcs represent protein cavities in which the adenine and 8-aryl moieties, respectively, bind. The three structural waters found in all Hsp90 structures are shown as blue circles. van der Waals interactions are indicated by blue arrowheads. (C) Comparison between **3** and **1** bound to Hsp90. Stereo diagram of hHsp90α−**3** (blue with green waters)(PDB code 1UYF) and Hsp90−**1** (white with red waters) interactions in the conformation specific binding channel. The gray water is a water observed in the other structures of 3′,4′,5′-trimethoxy purine scaffold inhibitors that is supported by the electron density but was not modeled in the hHsp90−**3** structure. The selected residues (Leu107, Phe138, Tyr139, and Trp162) surround the 8-aryl portion of these inhibitors and form the walls of the hydrophobic channel. The conformation of the 2′-chloro (yellow) in **3**, which places the 2′-halide above the adenine ring, is termed s-cis. The 2′-iodo (magenta) of **1** is rotated ∼180°, placing the 2′-halide away from the adenine ring in an s-trans conformation. An arrow indicates the ∼180° rotation of the 2′-halide from the s-trans of **1** to the s-cis of **3**.

accommodated differently than that of the 2′-halo-3′,4′,5′-trimethoxy series. Our structural results now confirm this hypothesis. As seen in Figure 2A and C, the 2′-iodo moiety of **1** in the complex with Hsp90 adopts an s-trans configuration. Compared to the s-cis 2′-chloro configuration seen in the

structure with **3**, which is one of the 2′-halo-3′,4′,5′-trimethoxy derivatives,[23] the 2′-iodo moiety is rotated nearly180° around the S−C1′ bond (Figure 2C).

The preference for the s-trans conformation of the 8-aryl group in the 2′-halo-4′,5′-methylenedioxy series compounds can

be ascribed to four factors. First, a systematic modeling of the rotation of the 8-aryl group made by incrementing the $\varphi 1$ and $\varphi 2$ dihedrals shows that the 8-aryl groups can only be accommodated within the ligand binding pocket in the s-cis or s-trans orientations. Intermediate orientations are disfavored because they would lead to clashes between the aryl group and Met98 and Phe138, two of the residues that line the ligand binding pocket. Second, the 4′,5′-methylenedioxy substituent has a fixed orientation relative to the 8-aryl ring, and only in the s-trans conformation does the bridging methylene group avoid steric clashes with Tyr139 in the ligand binding pocket. Such clashes are not observed in the 4′,5′-di- and 3′,4′,5′-trimethoxy series because the unlinked methoxy groups are independent of each other and are able to rotate away from the tyrosine ring. Third, the sulfur C8 linker found in **1** further disfavors the s-cis conformation because the bond angle for sulfur is more acute (~102°) compared to that of a methylene at the same position (~113°). The more acute sulfur angle would cause the interpenetration of the halide into the adenine ring were the 8-aryl group rotated into the s-cis conformation. Together, these last two points show that the conformation of the 8-aryl group and the position of the 2′-halide are pre-selected by the 4′,5′-methylenedioxy moiety and the sulfur linker. Finally, we note that the volume of the ligand binding pocket surrounding the 2′-halide in the s-trans conformation is larger than that available for the s-cis conformation, thus explaining the preference for the bulkier iodine in the 2′-halo-4′,5′-methylenedioxy series and the observed trend in activity (I > Br > Cl) for this series.[36]

Structural support for the proposal that larger 2′-halides improve binding affinity in the 2′-halo-4′,5′-methylenedioxy series comes from the structure of Hsp90 in complex with **2**. Compound **2** is identical to **1** except for a bromine in place of an iodine at the 2′ position. Compound **2** binds isosterically with **1** and adopts the s-trans conformation (not shown). The smaller bromine does not fill the C2′ pocket however, and an additional ordered water is observed trapped in the pocket (not shown). The entropy gained by the release of this water, in addition to the larger van der Waals interface for the iodine, may account for the greater affinity of **1** for Hsp90 compared to that of **2** for Hsp90.

Effect of Oxidation at the Sulfur Linker. The sulfur linker that bridges the C8 carbon of the adenine moiety to the 8-aryl ring can be modified by oxidation. It has been shown recently[35] that PU compounds such as **7** and **8** that contain sulfoxyl (−SO−) or sulfonyl (−SO$_2$−) linkers are significantly weaker inhibitors of Hsp90α than **6**, the corresponding sulfanyl (non-oxidized, −S−) ligand, as reported by EC$_{50}$ competition binding measurements and IC$_{50}$ assays of Her2 degradation in SKBr3 cells. To understand the cause of impaired binding, sulfoxyl-**2** and sulfonyl-**2** (Figure 3A) were modeled into the binding pocket of Hsp90. This analysis takes advantage of the structures of the complexes with **1** and **2** presented here, which are the first PU series compounds to have sulfur rather than methylene linkers and, thus, serve as experimentally observed starting points for modeling the oxidized sulfur compounds. These models show that the addition of an *S*-sulfoxyl, or sulfonyl-oxygens to **2** would lead to clashes with the Cβ of Phe138 (Figure 3A), thereby preventing binding. Because variations in the protein backbone in the vicinity of Phe138 have not previously been observed in the numerous Hsp90 *N*-domain structures solved to date, it is likely that the binding of these oxygenated derivatives would require a conformational rearrangement around the sulfur linker.

Insight into the minimum energy conformation of ligands oxygenated at the sulfur linker was gained by quantum chemical calculations on the model compound 8-phenylsulfanyl adenine (**9**, Figure 1C) and its oxygenated derivatives 8-phenylsulfoxyl adenine (**10**) (−SO−) and 8-phenylsulfonyl adenine (**11**) (−SO$_2$−). Interest in the minimum energy conformation stems from the previous observation that **4** derivatives tend to bind Hsp90 without internal rearrangment.[23] Compound **9** was chosen for this analysis because it contains all of the major substituents of **1** around the sulfur linkage. At the B3LYP/6-31G(d) level of theory, the energy-minimized conformation of **9**, determined after an exhaustive search of conformational space from multiple starting conformations (see Experimental Section), agreed well with the conformation of **1** observed here (Figure 3B). The observation that the minimum energy conformation of **9** mimics the crystallographically observed conformation of **1** suggests that the change from a −CH$_2$− linker to an −S− linker has not changed the preference for 8-aryl adenine inhibitors to bind without rearrangement.

To further test the validity of our comparisons between the quantum chemical energy optimized conformations and the conformation observed in our structures, a calculation on **2** was also performed. As seen in Figure 3D, the calculated conformation of **2**, which represents the convergence from multiple starting conformations, matches remarkably well with that seen in the Hsp90−**2** structure reported here.

Because the quantum calculations on the **9** and **2** returned low energy structures that agreed well with the observed structures of **1** and **2**, we next performed in vacuo quantum calculations to examine the effects of oxidation at the sulfur linker. As shown in Figure 3B and C, oxidation affects both dihedrals and the bond angle centered on the sulfur, but the most striking changes are to the dihedral on the benzene side. This dihedral, $\varphi 2$ (C8-S-C1′-C2′), decreases from 151° in the crystal structure of human Hsp90−PU-H64 to 96° in the optimized conformation of **11**. Interestingly, a histogram of the $\varphi 2$ dihedrals seen in similar substructures from the Cambridge Structural Database (CSD) yields a distribution that is centered around 85° (not shown). This large decrease in $\varphi 2$ turns the phenyl ring from nearly perpendicular to parallel with the C6−N6 bond (Figure 3B and C). This conformation would not only disrupt the face-on-face stacking of Phe138 with the model ligand but also lead to the interpenetration of the 8-aryl ring into Phe138 (Figure 3E). The binding of **10** or **11** would thus require a rearrangement of $\varphi 2$. In an attempt to quantify the energetic penalty of the rearrangement of $\varphi 2$ back to 151°, **10** or **11** were partially optimized holding $\varphi 2$ fixed at 151°. This analysis showed that the conformations of **10** or **11** with $\varphi 2$ fixed at 151° are disfavored by up to 5 kcal/mol compared to the fully optimized conformation. Flexibility within the binding pocket may decrease the energetic penalty of sulfoxyl or sulfonyl−**1** binding. Allowing for such considerations, the calculated energetic barrier is consistent with the observed 1−3 kcal/mol energy penalty inferred from EC$_{50}$ and IC$_{50}$ assays.[35]

Unique Interactions of the 3′,4′,5′-Trimethoxy Series. Besides oxidation at the sulfur linker, many other modifications of the 8-aryl adenine scaffold have also been explored. Among the first to be examined was the addition of 3′,4′,5′-trimethoxy groups to the 8-aryl moiety, which led to the discovery of **3**, the highest potency −CH$_2$− linked inhibitor with a 3′,4′,5′-trimethoxy modification.[25] Unlike **1**, **3** forms several hydrogen bonds in the 8-aryl binding pocket. These hydrogen bonds bridge the interaction between the 4′- and 5′-methoxy groups of **3** and the hydroxyl of Tyr139. Interestingly, a water in the ligand
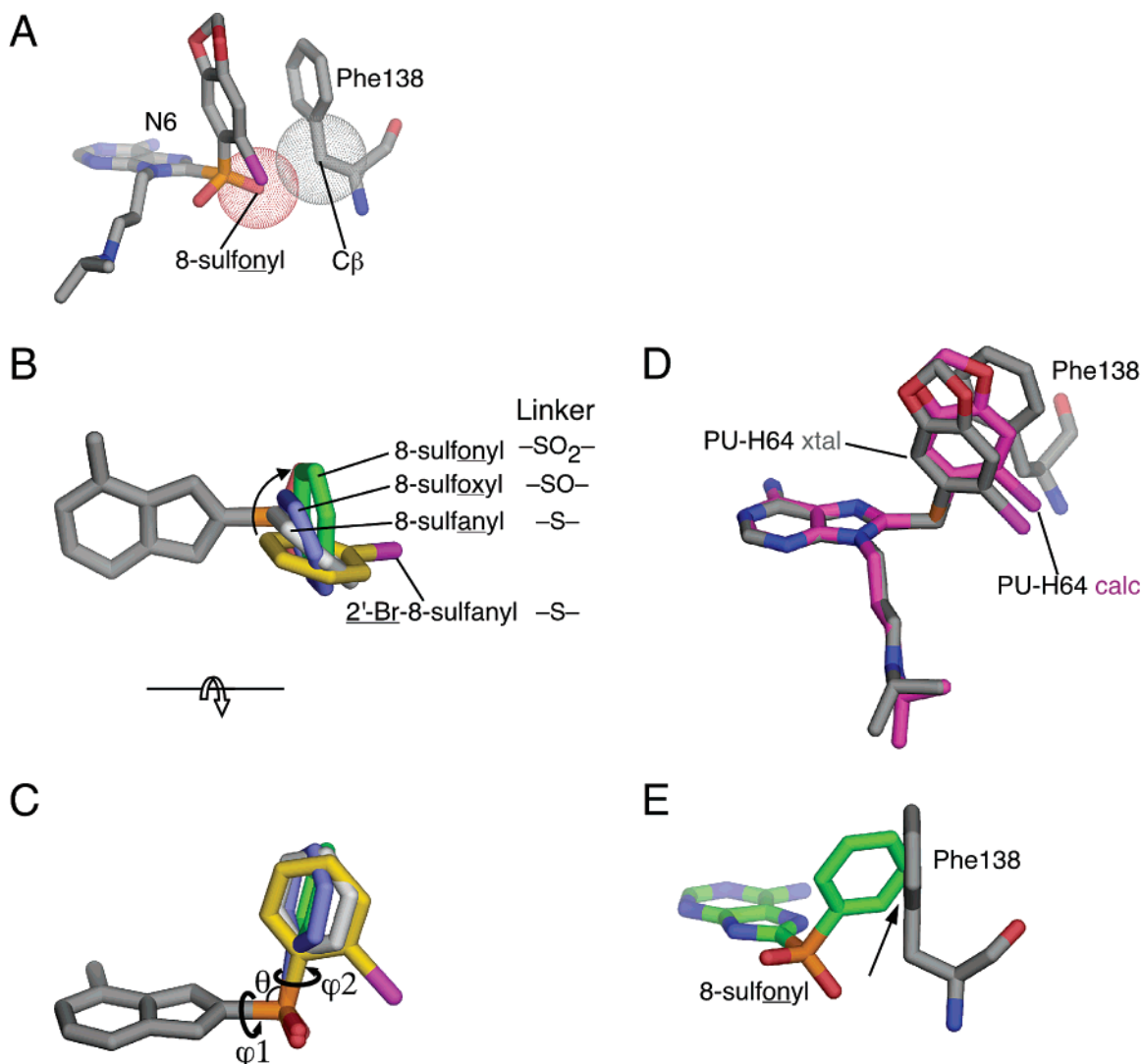
Figure 3. Calculated conformations of **2** and derivatives. (A) Model of the 8-sulfonyl derivative of **2** bound to Hsp90, showing potential clashes between one of the sulfonyl oxygens and the beta carbon of Phe138. van der Waals surfaces of the oxygen and beta carbon are shown as dots. (B) Overlay of the energy optimized conformations of 2′-bromo-8-sulfanyl-phenyl-adenine (gold) and 8-sulfanyl- (no oxidation of the sulfur; white), 8-sulfoxyl- (single oxidation of the sulfur; blue), and 8-sulfonyl-phenyl adenine (double oxidation of the sulfur; green) showing the rearrangement of $\varphi2$. Alignments for the ligands in (B), (C), and (D) overlaid the adenine moieties. (C) Same as (B), except rotated 90° around the horizontal axis. (D) Comparison of the energy optimized conformation of **2** (magenta) and the conformation observed experimentally in the crystal structure (gray). The calculated conformation is similar to that observed experimentally, thus supporting the validity of the energy minimization calculations. (E) The calculated low energy conformation of 8-phenylsulfanyl adenine, modeled into Hsp90. Phe138, which comprises the rear of the 8-aryl binding channel, is included to highlight the potential steric clashes that require the rearrangement of the model ligands for binding. Energy optimization was performed in Gaussian98 at the B3LYP/6-31G(d) level of theory.

binding pocket, which is observed in the **4**−Hsp90α complex but was left unmodeled in the complex with **3**, can be supported by the electron density calculated from the deposited structure factors for this complex. Considering this water (colored gray in Figure 2C) the hydrogen bonding network extends to include three waters that bridge the interactions between the 4′,5′-methoxy of **3**, the hydroxyl of Try139, and the polar nitrogen of the Trp162 side chain.

The hydrogen bonding network seen for the 8-aryl group of **3** seems to play an important role in the binding of the 3′,4′,5′-trimethoxy series inhibitors. This is highlighted by the observed shift in both the linker bond angle and the rotation of the φ (N9-C8-S-C1′) in the structures of 3′,4′,5′-trimethoxy series inhibitors in complex with Hsp90 compared to that of the other crystallographically observed −CH$_2$− linked PU inhibitors that lack the 3′,4′,5′-trimethoxy moiety. The linker bond angle in the 3′,4′,5′-trimethoxy series is ∼3° larger, and

the $\varphi1$ dihedral increases by ∼19° compared to that of the non-3′,4′,5′-trimethoxy compounds.

The changes around the linker also alter the trajectory of the 2′ substituent. For 2′-halo 3′,4′,5′-trimethoxy series inhibitors, the s-cis conformation provides additional room for the 2′-halide as a result of the increased bond angle and the rotated dihedral placing the halide further above and to the side of the adenine. In the s-trans conformation, the trajectory of the 2′-halide is positioned more along the edge of the pocket occupied by the 2′-iodo of **1** rather than down the center. Together, the more favorable trajectory of the 2′-halide in the s-cis compared to s-trans conformation and the desire to maintain the hydrogen binding network may explain the observed preference for 2′-halo 3′,4′,5′-trimethoxy series inhibitors binding in the s-cis conformation.

Quantum Calculations of a 4′,5′-Dimethoxy Compound. To probe the effects of a 4′,5′-dimethoxy modification to the

8-aryl adenine scaffold, quantum chemical calculations of the 2′-bromo-4′,5′-dimethoxy model compound **12** (8-(2′-bromo-4′,5′-dimethoxyphenylsulfanyl)-adenine) were performed. These calculations predict that the energy optimized conformation of the 8-aryl group in this compound would be nearly parallel to the C6−N6 bond with a $\varphi 2$ dihedral of ∼91°. This arrangement of the 8-aryl group is similar to that predicted for a sulfonyl (−SO$_2$−) linked 8-aryl adenine and would similarly result in clashes with Phe138. To gain insight into the energetic penalty paid during the rearrangement of to the of the 2′-bromo-4′,5′-dimethoxy model compound to the s-trans conformation, a partial optimization of **12** was performed while holding the $\varphi 2$ dihedral at 151°. These calculations showed that the s-trans conformation is disfavored by 3.0 kcal/mol, which is consistent with the 100-fold difference in IC$_{50}$ between the 4′,5′-dimethoxy and the 4′,5′-methylenedioxy series compounds.

Conclusion

Hsp90 inhibitors act as multitarget anti-cancer therapeutics by blocking the successful chaperoning of many oncogenic Hsp90 clients. The multitarget nature of Hsp90 inhibitors is more advantageous than single target drugs because of their applicability to a broader range of cancers. The development of efficacious anti-cancer therapeutics based on Hsp90 inhibitors requires an in-depth understanding of their mode of interaction and mechanism of inhibition. To this end, the experiments reported here dissect the mode of interaction and mechanism of inhibition of a novel water-soluble 8-aryl-sulfanyl adenine class of Hsp90 inhibitors. Our results present at atomic detail the structures of **1** and **2** bound to the isolated *N*-terminal domain of Hsp90α, highlighting critical conserved and novel interactions. These structures have also allowed us to perform quantum chemical calculations of 8-aryl-sulfanyl adenine derivatives that give insight into the effects of modification on this scaffold.

Experimental Procedures

Protein Expression and Purification. Human Hsp90 (1−236) was overexpressed in *E. coli* as an amino-terminal hexa-Histidine tagged protein. This construct was purified by Ni-NTA agarose affinity chromatography followed by dialysis, ion exchange chromatography on Q-sepharose (pH 8.0), and gel filtration chromatography on S-200. The purified protein was concentrated to 20 mg/mL in preparation for crystallization. Compounds **1** and **2** were synthesized as previously reported.[35]

Crystallization of Hsp90−PU Ligand Complexes. Crystals of human Hsp90α in complex with **1** or **2** were grown at 4 °C by hanging drop vapor diffusion. Hanging drops contained ∼4 mM ligand (a 5-fold molar excess) and a 1:1 ratio of protein (20 mg/mL Hsp90 in 10 mM Tris at pH 7.6, 100 mM NaCl, 1 mM DTT) to reservoir (100 mM Na cacodylate at pH 6.5, 200−250 mM MgCl$_2$, 10−12% w/v PEG 2000 monomethyl ether). Crystals with a typical edge length of 200 μm appeared after 1−2 days. The crystals were harvested and cryo-protected in nylon loops by a quick swish through the reservoir solution followed by a second pass through 35% PEG 2000 MME, 100 mM Na cacodylate at pH 6.5, and 200 mM MgCl$_2$. Directly following cryo-protection, the crystals were flash cooled in liquid nitrogen. The crystals of yeast Hsp90 in complex with **2** were grown at 18 °C in a similar manner, except that the protein concentration was 33 mg/mL, the reservoir contained 200 mM ammonium dihydrogen phosphate at pH 4.6 and 20% w/v PEG 3350, and the crystals were cryo-protected by passage through 50% glycerol, 100mM magnesium acetate and 10% w/v PEG 3350.

Data Collection, Structure Determination, and Refinement. Atomic resolution data for the crystals of human Hsp90α with bound **1** and **2** were collected on an Raxis IV detector using an RU-H3R generator and Osmic Mirrors. Data reduction and scaling was performed using XDS.[37] The initial phases for the complex of **2** with Hsp90 were obtained using molecular replacement (MolRep) with PDB entry 1UY6 as the search model. SAD phases for the complex with **1** were obtained from the strong anomalous signal of the single iodine atom on the ligand and were of sufficient quality to produce readily interpretable maps. The molecular replacement and following intermediate models were refined iteratively by manual rebuilding in O and refinement in CNS.[38,39] The placement of **2** and solvent molecules was determined by the use of overlapping peaks of difference and simulated annealing omit density. Parameter and topology files for **1** and **2** were generated using the Dundee PRODRG server.[40] In later rounds of refinement, ligand dihedral constraints were relaxed, alternate conformations were added, and restrained individual B-factors were used. Structure validation was performed using KiNG and MolProbity.[41,42] The structure of yeast Hsp90 in complex with **2** was solved by molecular replacement using PDB entry 1AH6 as the search model[43,44] and refined in a similar manner. Data collection and refinement statistics are shown in Table 2. Molecular graphics were created using Pymol (DeLano Scientific, South San Francisco, CA).

Coordinates. Structure factors and coordinates have been deposited in the PDB.[45] The corresponding PDB code for these structures are 2FWY (human Hsp90α−**2**), 2FWZ (human Hsp90α−**1**), and 1ZW9 (yeast Hsp90−**2**).

Quantum Chemical Calculations. The geometry of the model compounds **9**, **10**, and **11** were optimized using Gaussian 98 (Gaussian, Inc., Wallingford, CT) at the B3LYP/6-31G(d) level of theory. To ensure that the optimizations predicted a global minimum, a relaxed 12 × 12 degree potential energy surface (PES) scan of $\varphi 1$ and $\varphi 2$ was preformed at the Hartree−Fock/STO-3G level of theory. In addition to the relaxed PES scan, each optimization was preformed starting from an ensemble of initial conformations, which typically included at least one starting orientation of the 8-aryl group that was 180° opposed in $\varphi 1$ from the observed conformation, to ensure that the highest energy barrier was overcome in the search for the low energy conformation. In all cases, the optimizations predicted the same low energy conformation. These data agreed well with the global minimum found in the relaxed PES scan.

When comparing the geometry optimized conformation of **10** or **11** to the conformation adopted by **9**, the dihedrals and bond angle around the sulfur position were varied individually while keeping the other angles in their energy optimized conformation. The total change in energy for **10** or **11** when being constrained to the conformation of the sulfanyl compound **9** was taken as the sum of the individual differences. Calculations were performed in vacuo to allow for reasonable computation times.

References

(1) Maloney, A.; Workman, P. HSP90 as a new therapeutic target for cancer therapy: the story unfolds. *Expert Opin. Biol. Ther.* **2002**, *2*, 3−24.

(2) Pearl, L. H. Hsp90 and Cdc37−a chaperone cancer conspiracy. *Curr. Opin. Genet. Dev.* **2005**, *15*, 55−61.

(3) McLaughlin, S. H.; Ventouras, L. A.; Lobbezoo, B.; Jackson, S. E. Independent ATPase activity of Hsp90 subunits creates a flexible assembly platform. *J. Mol. Biol.* **2004**, *344*, 813−826.

(4) Richter, K.; Walter, S.; Buchner, J. The Co-chaperone Sba1 connects the ATPase reaction of Hsp90 to the progression of the chaperone cycle. *J. Mol. Biol.* **2004**, *342*, 1403−1413.

(5) Dollins, D. E.; Immormino, R. M.; Gewirth, D. T. Structure of unliganded GRP94, the endoplasmic reticulum Hsp90: Basis for nucleotide-induced conformational change. *J. Biol. Chem.* **2005**, *280*, 30438−30447.

(6) Immormino, R. M.; Dollins, D. E.; Shaffer, P. L.; Soldano, K. L.; Walker, M. A.; et al. Ligand-induced conformational shift in the N-terminal domain of GRP94, an Hsp90 chaperone. *J. Biol. Chem.* **2004**, *279*, 46162−46171.

(7) Prodromou, C.; Roe, S. M.; O'Brien, R.; Ladbury, J. E.; Piper, P. W.; et al. Identification and structural characterization of the ATP/ADP-binding site in the Hsp90 molecular chaperone. *Cell* **1997**, *90*, 65−75.

(8) Marcu, M. G.; Chadli, A.; Bouhouche, I.; Catelli, M.; Neckers, L. M. The heat shock protein 90 antagonist novobiocin interacts with a previously unrecognized ATP-binding domain in the carboxyl terminus of the chaperone. *J. Biol. Chem.* **2000**, *275*, 37181−37186.

(9) Cliff, M. J.; Williams, M. A.; Brooke-Smith, J.; Barford, D.; Ladbury, J. E. Molecular recognition via coupled folding and binding in a TPR domain. *J. Mol. Biol.* **2005**, *346*, 717−732.

(10) Pratt, W. B. The hsp90-based chaperone system: involvement in signal transduction from a variety of hormone and growth factor receptors. *Proc. Soc. Exp. Biol. Med.* **1998**, *217*, 420−434.

(11) Huai, Q.; Wang, H.; Liu, Y.; Kim, H. Y.; Toft, D.; et al. Structures of the N-terminal and middle domains of E. coli Hsp90 and conformation changes upon ADP binding. *Structure (London)* **2005**, *13*, 579−590.

(12) Meyer, P.; Prodromou, C.; Hu, B.; Vaughan, C.; Roe, S. M.; et al. Structural and functional analysis of the middle segment of hsp90. Implications for ATP hydrolysis and client protein and cochaperone interactions. *Mol. Cell* **2003**, *11*, 647−658.

(13) Chiosis, G.; Vilenchik, M.; Kim, J.; Solit, D. Hsp90: the vulnerable chaperone. *Drug Discovery Today* **2004**, *9*, 881−888.

(14) Pratt, W. B.; Toft, D. O. Regulation of signaling protein function and trafficking by the hsp90/hsp70-based chaperone machinery. *Exp. Biol. Med. (Maywood, NJ, U.S.)* **2003**, *228*, 111−133.

(15) Shao, J.; Grammatikakis, N.; Scroggins, B. T.; Uma, S.; Huang, W.; et al. Hsp90 regulates p50(cdc37) function during the biogenesis of the activeconformation of the heme-regulated eIF2 alpha kinase. *J. Biol. Chem.* **2001**, *276*, 206−214.

(16) Schulte, T. W.; An, W. G.; Neckers, L. M. Geldanamycin-induced destabilization of Raf-1 involves the proteasome. *Biochem. Biophys. Res. Commun.* **1997**, *239*, 655−659.

(17) Chiosis, G.; Timaul, M. N.; Lucas, B.; Munster, P. N.; Zheng, F. F.; et al. A small molecule designed to bind to the adenine nucleotide pocket of Hsp90 causes Her2 degradation and the growth arrest and differentiation of breast cancer cells. *Chem. Biol.* **2001**, *8*, 289−299.

(18) Matsumoto, Y.; Machida, H.; Kubota, N. Preferential sensitization of tumor cells to radiation by heat shock protein 90 inhibitor geldanamycin. *J. Radiat. Res. (Tokyo)* **2005**, *46*, 215−221.

(19) Sausville, E. A.; Tomaszewski, J. E.; Ivy, P. Clinical development of 17-allylamino, 17-demethoxygeldanamycin. *Curr. Cancer Drug Targets* **2003**, *3*, 377−383.

(20) Blagosklonny, M. V.; Fojo, T.; Bhalla, K. N.; Kim, J. S.; Trepel, J. B.; et al. The Hsp90 inhibitor geldanamycin selectively sensitizes Bcr-Abl-expressing leukemia cells to cytotoxic chemotherapy. *Leukemia* **2001**, *15*, 1537−1543.

(21) Neckers, L.; Schulte, T. W.; Mimnaugh, E. Geldanamycin as a potential anti-cancer agent: its molecular target and biochemical activity. *Invest. New Drugs* **1999**, *17*, 361−373.

(22) Schulte, T. W.; Akinaga, S.; Soga, S.; Sullivan, W.; Stensgard, B.; et al. Antibiotic radicicol binds to the N-terminal domain of Hsp90 and shares important biologic activities with geldanamycin. *Cell Stress Chaperones* **1998**, *3*, 100−108.

(23) Wright, L.; Barril, X.; Dymock, B.; Sheridan, L.; Surgenor, A.; et al. Structure-activity relationships in purine-based inhibitor binding to HSP90 isoforms. *Chem. Biol.* **2004**, *11*, 775−785.

(24) Chiosis, G.; Timaul, M. N.; Lucas, B.; Munster, P. N.; Zheng, F. F.; et al. A small molecule designed to bind to the adenine nucleotide pocket of Hsp90 causes Her2 degradation and the growth arrest and differentiation of breast cancer cells. *Chem. Biol.* **2001**, *8*, 289−299.

(25) Vilenchik, M.; Solit, D.; Basso, A.; Huezo, H.; Lucas, B.; et al. Targeting wide-range oncogenic transformation via PU24FCl, a specific inhibitor of tumor Hsp90. *Chem. Biol.* **2004**, *11*, 787−797.

(26) Chiosis, G.; Lucas, B.; Shtil, A.; Huezo, H.; Rosen, N. Development of a purine-scaffold novel class of Hsp90 binders that inhibit the proliferation of cancer cells and induce the degradation of Her2 tyrosine kinase. *Bioorg. Med. Chem.* **2002**, *10*, 3555−3564.

(27) Biamonte, M. A.; Shi, J.; Hong, K.; Hurst, D. C.; Zhang, L.; et al. Orally active purine-based inhibitors of the heat shock protein 90. *J. Med. Chem.* **2006**, *49*, 817−828.

(28) Kamal, A.; Thao, L.; Sensintaffar, J.; Zhang, L.; Boehm, M. F.; et al. A high-affinity conformation of Hsp90 confers tumour selectivity on Hsp90 inhibitors. *Nature* **2003**, *425*, 407−410.

(29) Dymock, B. W.; Barril, X.; Brough, P. A.; Cansfield, J. E.; Massey, A.; et al. Novel, potent small-molecule inhibitors of the molecular chaperone Hsp90 discovered through structure-based design. *J. Med. Chem.* **2005**, *48*, 4212−4215.

(30) Shen, G.; Blagg, B. S. Radester, a novel inhibitor of the Hsp90 protein folding machinery. *Org. Lett.* **2005**, *7*, 2157−2160.

(31) Clevenger, R. C.; Blagg, B. S. Design, synthesis, and evaluation of a radicicol and geldanamycin chimera, radamide. *Org. Lett.* **2004**, *6*, 4459−4462.

(32) Cheung, K. M.; Matthews, T. P.; James, K.; Rowlands, M. G.; Boxall, K. J.; et al. The identification, synthesis, protein crystal structure and in vitro biochemical evaluation of a new 3,4-diarylpyrazole class of Hsp90 inhibitors. *Bioorg. Med. Chem. Lett.* **2005**, *15*, 3338−3343.

(33) Kreusch, A.; Han, S.; Brinker, A.; Zhou, V.; Choi, H. S.; et al. Crystal structures of human HSP90alpha-complexed with dihydroxyphenyl-pyrazoles. *Bioorg. Med. Chem. Lett.* **2005**, *15*, 1475−1478.

(34) Chene, P. ATPases as drug targets: learning from their structure. *Nat. Rev. Drug Discovery* **2002**, *1*, 665−673.

(35) Llauger, L.; He, H.; Kim, J.; Aguirre, J.; Rosen, N.; et al. Evaluation of 8-arylsulfanyl, 8-arylsulfoxyl, and 8-arylsulfonyl adenine derivatives as inhibitors of the heat shock protein 90. *J. Med. Chem.* **2005**, *48*, 2892−2905.

(36) He, H.; Zatorska, D.; Kim, J.; Aguirre, J.; Llauger, L.; et al. Identification of potent water soluble purine-scaffold inhibitors of the heat shock protein 90. *J. Med. Chem.* **2006**, *49*, 381−390.

(37) Kabsch, W. Automatic processing of rotation diffraction data from crystals of initially unknown symmetry and cell constants. *J. Appl. Crystallogr.* **1993**, *26*, 795−800.

(38) Jones, T. A.; Zou, J. Y.; Cowan, S. W.; Kjeldgaard, M. Improved methods for binding protein models in electron density maps and the location of errors in these models. *Acta Crystallogr., Sect. A* **1991**, *47*, 110−119.

(39) Brunger, A. T.; Adams, P. D.; Clore, G. M.; DeLano, W. L.; Gros, P.; et al. Crystallography & NMR system: A new software suite for macromolecular structure determination. *Acta Crystallogr., Sect. D* **1998**, *54*, 905−921.

(40) Schuttelkopf, A. W.; van Aalten, D. M. PRODRG: a tool for high-throughput crystallography of protein−ligand complexes. *Acta Crystallogr., Sect. D* **2004**, *60*, 1355−1363.

(41) Richardson, J. S.; Arendall, W. B., 3rd; Richardson, D. C. New Tools and Data for Improving Structures, Using All-Atom Contacts. *Methods in Enzymology*; Academic Press: San Diego, CA, 2003; pp 385−412.

(42) Lovell, S. C.; Davis, I. W.; Arendall, W. B., 3rd; de Bakker, P. I.; Word, J. M.; et al. Structure validation by Calpha geometry: phi, psi and Cbeta deviation. *Proteins* **2003**, *50*, 437−450.

(43) Vagin, A.; Teplyakov, A. MOLREP: an automated program for molecular replacement. *J. Appl. Crystallogr.* **1997**, *30*, 1022−1025.

(44) Prodromou, C.; Roe, S. M.; Piper, P. W.; Pearl, L. H. A molecular clamp in the crystal structure of the N-terminal domain of the yeast Hsp90 chaperone. *Nat. Struct. Biol.* **1997**, *4*, 477−482.

(45) Berman, H. M.; Bhat, T. N.; Bourne, P. E.; Feng, Z.; Gilliland, G.; et al. The Protein Data Bank and the challenge of structural genomics. *Nat. Struct. Biol.* **2000**, *7*, 957−959.